ELECTROSTATIC MODELING OF IN-PLANE OVERLAP ENERGY HARVESTERS

Cuong Phu Le and Einar Halvorsen
Institute for Microsystem Technology, Vestfold University College, Norway

Abstract: A technique to calculate the capacitance matrix of in-plane overlap plate transducers is described in this paper. The investigated electrostatic transducers have metal strip electrodes where fringing fields have a significant effect on the capacitance variation. We also take into account end effects and a nearby ground plane. The technique is used for modeling and simulation of electrostatic energy harvesters which have a charged floating electrode. We find that the device performance strongly depends on the interplay between the amount of trapped charge and the acceleration amplitude. The fringing field effects cause a substantially reduced output power compared to that obtained from the parallel plate model for the same electrode geometry. The negative effects of the fringing fields can be reduced by optimization of the metal finger widths. The optimum is different from that of the parallel plate model and is also dependent on the acceleration amplitude.

Keywords: energy harvester, electrostatic transducer, variable capacitance and fringing fields.

INTRODUCTION

Energy harvesting from motion is a promising alternative to batteries as a power source for wireless, autonomous devices. This contribution focuses on electrostatic energy harvesters; other commonly studied alternatives are piezoelectric and electromagnetic devices. Typically, but not always, an electrostatic harvester is based on a variable capacitance which may come in a variety of configurations. The capacitance variation results from the motion of an electrode located on a proof mass relative to a fixed electrode [1]. This work focuses on electrostatic energy harvester modeling with in-plane overlap electrode structure (IPOP), consisting of a metal strip set on two layer dielectrics opposing each other. The approach is similar to that used for micro strip lines [2] and surface acoustic wave devices [3]. The electrode gap is small compared to metal strip dimensions and considerable capacitive coupling to the back side of electrode stripes may occur. Therefore, fringing fields must be taken into account in the variable capacitance calculation. In addition, we also consider a non-periodic charge distribution and the presence of a nearby ground plane. This contribution differs from our own previous work [4] in giving the analytical formulation for all these effects, in applying the result to a floating electrode device, and in demonstrating significant performance consequences of fringing fields in this type of device.

The charge distribution on each metal strip is expanded in Chebyshev polynomials multiplied by a reciprocal square root form. The charge distributions near end strips will differ from those in the middle so we use different expansion coefficients for different metal strips. The expansion captures both edge singularities and end effects. The Galerkin method is used to enforce potential boundary conditions to obtain expansion coefficients. Thus, the capacitance matrix is determined. The analytical formulation is then applied to an electrostatic transducer model with an upper floating electrode that is pre-charged. The model is implemented in a SPICE simulator and includes stoppers to limit mass motion. The fringing fields have considerable effects on the capacitance matrix and the obtained output power compared to an otherwise identical compact model built on the parallel-plate capacitor formula.

ANALYSIS

Electrostatic transducer structure

The electrostatic structure consists of *(2M+1)* metal microstrip pairs on two opposing dielectrics with permittivity of ε_1 and ε_2 for upper and lower electrodes respectively, see Fig. 1. The two set of metal strips are considered as zero thickness perfect conductors and are periodically laid on the dielectrics with pitch p. An upper/lower m^{th}-metal strip has a width $a_m^{U/L}$ and a length L. Two electrodes are separated by a gap g with permittivity ε_0 of the medium. A ground plane is located above the upper dielectric layer at a distance d. The upper electrode acts as a counter electrode moving in the horizontal direction with relative displacement b to the base electrode.

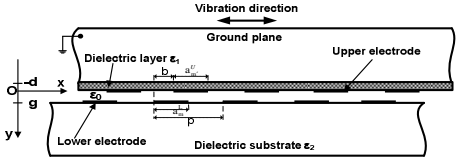

Fig. 1: Cross section of the electrostatic structure

Mathematical formulation

Chebyshev polynomials $T_n(x)$ multiplied by a reciprocal square root form express the charge distribution by inclusion of both edge singularities on each metal strip, see [2-3]. The charge distributions on the metal strips near the ends differ from those in the middle due to the different coupling to their neighbors. Therefore, a separate set of expansion coefficients $\{C_{mn}^{U/L}\}$ determine the charge distribution of the m^{th} strip of the upper/lower electrodes. Thus, the entire charge distribution can be written

$$\sigma^{U/L}(x)=\sum_{mn}C_{mn}^{U/L}\frac{T_n(\frac{2(x-mp-b^{U/L})}{a_m^{U/L}})}{\sqrt{1-\frac{4(x-mp-b^{U/L})^2}{(a_m^{U/L})^2}}}\theta(\frac{(a_m^{U/L})^2}{4}-(x-mp-b^{U/L})^2) \quad (1)$$

where,

$$\theta(x)=\begin{cases}1 & x\ge 0\\ 0 & x<0\end{cases} \text{ and } \begin{cases}b^{U/L}=b & \text{for the upper electrode}\\ b^{U/L}=0 & \text{for the lower electrode}\end{cases}$$

An analysis of electric fields based on the Laplace equation and the boundary condition for the potential $\varphi(x,y)$ is used to determine the Green functions g^{UU}, g^{UL}, g^{LU} and g^{LL} such that

$$\varphi^{U/L}(x)=\int_{-\infty}^{+\infty}g^{UU/LU}(x-x')\sigma^{U}(x)dx'+\int_{-\infty}^{+\infty}g^{UL/LL}(x-x')\sigma^{L}(x)dx' \quad (2)$$

In order to calculate the variable capacitance, the expansion coefficients $\{C_{mn}^{U/L}\}$ must be found. We use the Galerkin method with the reciprocal square root form as a weight function. The constant potential $V_m^{U/L}$ on each metal microstrip can be represented in terms of Chebyshev polynomials multiplied by expansion coefficients $\{\varphi_{mn}^{U/L}\}$ as

$$\varphi^{U/L}(x)=\sum_m V_m^{U/L}\theta(\frac{(a_m^{U/L})^2}{4}-(x-mp-b^{U/L})^2)=\sum_{mn}\varphi_{mn}^{U/L}u_{mn}^{U/L}(x) \quad (3)$$

where,

$$u_{mn}^{U/L}(x)=\sqrt{\frac{2}{a_m^{U/L}h_n}}T_n\left(\frac{x-mp-b^{U/L}}{a_m^{U/L}/2}\right)\theta(1-\frac{4}{(a_m^{U/L})^2}(x-mp-b^{U/L})^2)$$

By enforcing the potential boundary condition for each metal strip, the expansion coefficients $\{\varphi_{mn}^{U/L}\}$ are found by calculating the following inner products

$$\varphi_{mn}^{U/L}=\int_{-\infty}^{+\infty}\psi_{mn}^{U/L}\varphi^{U/L}(x)dx=\sqrt{\frac{h_0a_m^{U/L}}{2}}V_m^{U/L}\delta_{n,0} \quad (4)$$

where,

$$\psi_{mn}^{U/L}(x)=\frac{u_{mn}^{U/L}(x)}{\sqrt{1-\frac{4}{(a_m^{U/L})^2}(x-mp-b^{U/L})^2}},\ h_n=\begin{cases}\pi & n=0\\ \frac{\pi}{2} & n\ne 0\end{cases} \text{ and } \delta_{n,0}=\begin{cases}1 & n=0\\ 0 & n\ne 0\end{cases}$$

Substituting (1-3) into (4) leads to

$$\varphi_{mn}^{U/L}=\sum_{m'n'}\int_{-\infty}^{+\infty}\int_{-\infty}^{+\infty}\psi_{mn}^{U/L}(x)g^{UU/LU}(x-x')\psi_{m'n'}^{U}(x')dxdx'C_{m'n'}^{U}+ \\ +\sum_{m'n'}\int_{-\infty}^{+\infty}\int_{-\infty}^{+\infty}\psi_{mn}^{U/L}(x)g^{UL/LL}(x-x')\psi_{m'n'}^{L}(x')dxdx'C_{m'n'}^{L} \quad (5)$$

Finally, we obtain a set of equations for the expansion coefficients:

$$\sqrt{\frac{h_0a_m^{U/L}}{2}}V_m^{U/L}\delta_{n,0}=\sum_{m'n'}G_{mn;m'n'}^{UU/LU}C_{m'n'}^{U}+\sum_{m'n'}G_{mn;m'n'}^{UL/LL}C_{m'n'}^{L} \quad (6)$$

The system of equations (6) can be organized on a matrix form with a composition of submatrices as

$$\begin{bmatrix}\mathbf{G_{00}^{UU}} & \mathbf{G_{01}^{UU}} & \mathbf{G_{00}^{UL}} & \mathbf{G_{01}^{UL}}\\ \mathbf{G_{10}^{UU}} & \mathbf{G_{11}^{UU}} & \mathbf{G_{10}^{UL}} & \mathbf{G_{11}^{UL}}\\ \mathbf{G_{00}^{LU}} & \mathbf{G_{01}^{LU}} & \mathbf{G_{00}^{LL}} & \mathbf{G_{01}^{LL}}\\ \mathbf{G_{10}^{LU}} & \mathbf{G_{11}^{LU}} & \mathbf{G_{10}^{LL}} & \mathbf{G_{11}^{LL}}\end{bmatrix}\begin{bmatrix}\mathbf{C_0^U}\\ \mathbf{C_1^U}\\ \mathbf{C_0^L}\\ \mathbf{C_1^L}\end{bmatrix}=\begin{bmatrix}V^U\boldsymbol{\lambda}_\mathbf{0}^\mathbf{U}\\ \mathbf{0}\\ V^L\boldsymbol{\lambda}_\mathbf{0}^\mathbf{L}\\ \mathbf{0}\end{bmatrix} \quad (7)$$

where,

$$\left[\mathbf{C_0^{U/L}}\right]_{m'+M+1}=C_{m'0}^{U/L},\ \left[\mathbf{C_1^{U/L}}\right]_{m'+n'+M(n'\ne 0)}=C_{m'n'}^{U/L},\ \left[\boldsymbol{\lambda}_\mathbf{0}^\mathbf{U/L}\right]_{m+M+1}=\sqrt{\frac{h_0a_m^{U/L}}{2}}\frac{V_m^{U/L}}{V^{U/L}}$$

The total charges on the upper/lower electrodes can be expressed in terms of $\mathbf{C_0^U}$ and $\mathbf{C_0^L}$ as

$$Q^{U/L}=\boldsymbol{\nu}_\mathbf{0}^\mathbf{U/L}\mathbf{C_0^{U/L}} \qquad \left[\boldsymbol{\nu}_\mathbf{0}^\mathbf{U/L}\right]_m=\sqrt{\frac{h_0a_m^{U/L}}{2}} \quad (8)$$

Finally, the relationship between the total upper/lower charges and the upper/lower potentials is found by elimination of unknowns and represented by a capacitance coefficient matrix as

$$\begin{bmatrix}Q^U\\ Q^L\end{bmatrix}=\begin{bmatrix}C^{UU}(b) & C^{UL}(b)\\ C^{LU}(b) & C^{LL}(b)\end{bmatrix}\begin{bmatrix}V^U\\ V^L\end{bmatrix} \quad (9)$$

The capacitance coefficient matrix depends on the displacement b. It has two coefficients of "upper/lower capacitance" $C^{UU/LL}$ and a coefficient of induction $C^{UL}=C^{LU}$ for the coupling between the electrodes.

Charge distribution

For numerical investigations, we consider a structure with 39 metal strip pairs of width $a_m^U=a_m^L=50\mu m$ and length L=4mm. The metallization ratio is the ratio of the metal strip width $a_m^{U/L}$ to the finger pitch p=100μm. The upper electrode is on a silicon dioxide layer with thickness d=2μm deposited on the silicon mass which is grounded. The lower electrode on the glass substrate is separated from the upper electrode by a gap g=3μm.

The resulting charge distribution significantly depends on the potential on each electrode relative to ground plane. In the fig. 2, the lower charge on the middle and the edge are negative for V^U=5V at b=0. The presence of the ground plane causes positive

charge on the edge regions for V^U=2V. Moreover, the end effects are evident through the difference between the charge distributions on the middle and end strips, especially at their edges.

DEVICE MODEL

The capacitance calculation is applied to an energy harvester model with the upper floating electrode having a constant charge Q^U=Q_b to provide a bias (Fig. 3). The silicon proof mass has a total size of 3.9x4mm^2 and m=18.6mg. Spring stiffness is designed for natural frequency f_0=1200Hz and mechanical quality factor is Q_F=500. A lumped model of the electrostatic transducer is implemented in SPICE. The equivalent circuit includes stoppers to confine the proof mass movement. Output power is simply evaluated from the output voltage across the connected load resistance R_L.

A maximum output power of about 0.38µW is achieved at the load resistance R_L=2MΩ for an acceleration of 0.5g, a fixed charge Q_b=2nC and a vibration frequency f_0=1200Hz. Fig. 4 illustrates the influence of bias charge and acceleration on output power. For a particular acceleration, there is an optimal bias charge that maximizes the output power. Though output power first increases with the amount of charge, the higher electrostatic force eventually results in restriction of the mass motion and a corresponding drop of output power. A sufficiently large acceleration amplitude a_e is able to drive the pr-

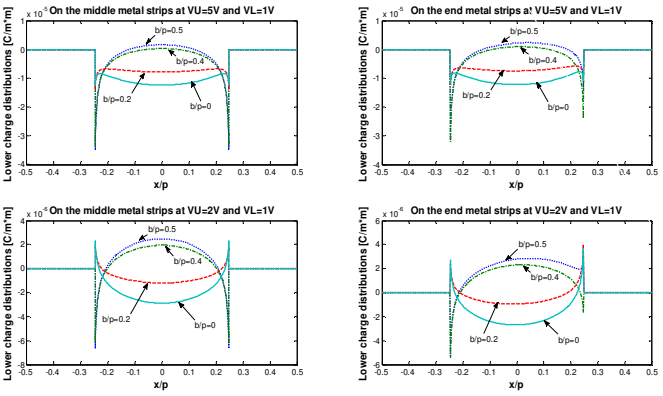

Fig. 2: Charge distributions on middle and end strips for V^U=5V, V^U=2V and V^L=1V

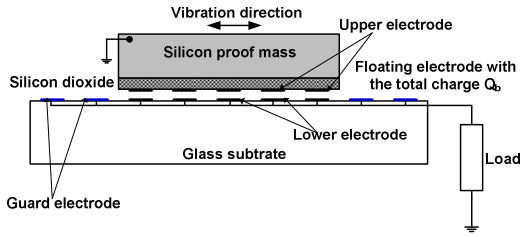

Fig. 3: Cross section of electrostatic harvester with upper floating electrode as total charge bias Q_b

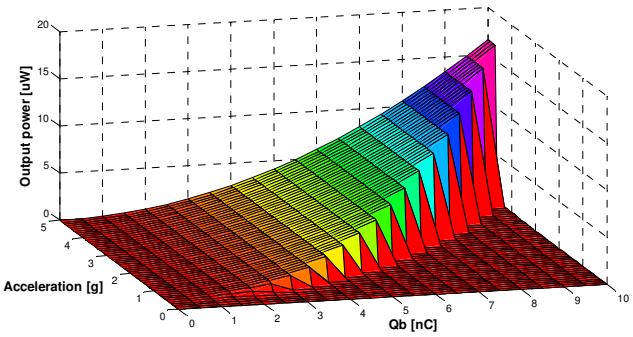

Fig. 4: Output power as a function of acceleration and bias charge at R_L=2MΩ, Q_F=500 and f_0=1200Hz

-oof mass into impact on the stoppers for any given bias charge, leading to saturated output power.

COMPARISON WITH PARALLEL PLATE MODEL

Using a parallel plate model, the electrostatic transducer can be represented by three capacitances $C^{LG}(b)$, $C^{UG}(b)$ and $C^{LUG}(b)$ connected as in fig. 5. From Table 2, the capacitance and induction coefficients with fringing fields are generally larger than those without fringing fields. These differences become bigger for smaller gap size, meaning that the fringing field effects become substantial. The coefficient differences between the parallel plate model and the one with fringing fields can be thought of as additional fringing capacitances. They vary with the relative displacement b.

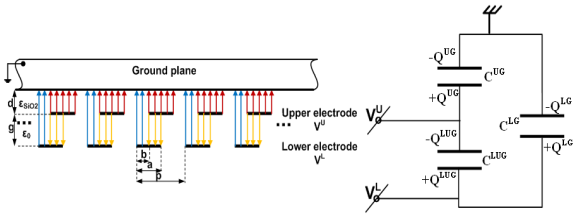

Fig. 5: Parallel plate model for electrostatic design

Table 2: Comparison of coefficients with and without fringing fields

With fringing fields						
Gap	C^{UU} [pF]		$-C^{UL}=-C^{LU}$ [pF]		C^{LL} [pF]	
	Max	Min	Max	Min	Max	Min
g=1µm	209.4	155.4	70.2	16.6	82.2	61.2
g=3µm	163.6	150.5	23.5	10.5	32.4	29.8
g=5µm	154.6	148.5	14.2	8.0	21.2	20.4
g=10µm	148.1	146.2	7.1	5.2	12.0	11.8
Without fringing fields						
Gap	C_{pp}^{UU} [pF]		$-C_{pp}^{UL}=-C_{pp}^{LU}$ [pF]		C_{pp}^{LL} [pF]	
	Max	Min	Max	Min	Max	Min
g=1µm	203.7	134.7	69.1	0	69.1	45.6
g=3µm	157.7	134.7	23.0	0	23.0	19.6
g=5µm	148.5	134.7	13.8	0	13.8	12.5
g=10µm	141.6	134.7	6.9	0	6.9	6.5

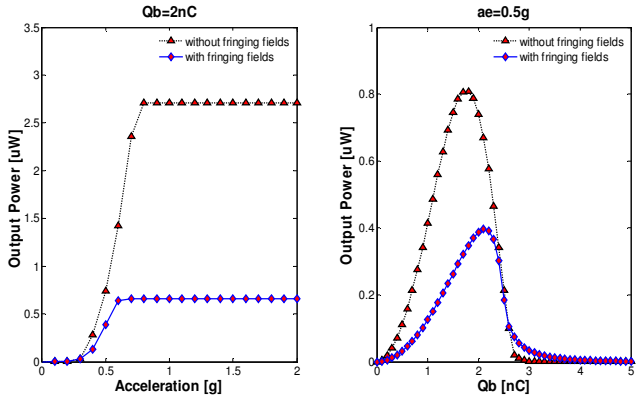

Fig. 6: Output power as a function of acceleration and bias charge for R_L=2MΩ, Q_F=500 and f_0=1200Hz

Based on the parallel plate model in fig. 5, the upper capacitance coefficient C_{pp}^{UU} is limited by a value of 134.7pF as the gap g approaches infinity. The limiting value of this coefficient is approximately 141pF with fringing fields.

Fig. 6 shows a comparison of output power as a function of acceleration a_e and bias charge Q_b with and without fringing fields. Less output is obtained for the model with fringing fields than for the parallel plate model. From the left of fig.6, the electrostatic damping force in the parallel plate model is bigger than that of the model with fringing fields at the same acceleration. With fringing fields, the mass reaches the stoppers at the acceleration amplitude a_e=0.6g giving the saturated output power of 0.6μW. For the parallel plate model, the corresponding values are 0.8g and 2.7μW. At a_e=0.5g, a maximum output power of 0.4μW can be achieved for the optimal bias charge Q_b=2.1nC when fringing fields are accounted for. In the parallel plate model, the optimum value is about 0.8μW for Q_b=1.7nC. Further increase of the bias charge causes reduced proof mass motion, ultimately resulting in smaller output power than that with fringing fields.

The fringing field effects are pronounced when varying the lower metallization ratio a^L/p while keeping the upper metallization ratio a^U/p=0.5 fixed. At the same metallization ratio, the larger capacitance and induction coefficient differences in the parallel plate model result in higher output power than with fringing fields. The optimal metallization ratio depends on the excitation level, for example a_e=1g, a^L/p=0.4 for the parallel plate model giving an output power of 2.9μW. With fringing fields, the optimum is a^L/p=0.3 which gives 1.5μW. The output power becomes very small for a^L/p approaching 0 or 1 due to decreased variations of the capacitance and induction coefficients.

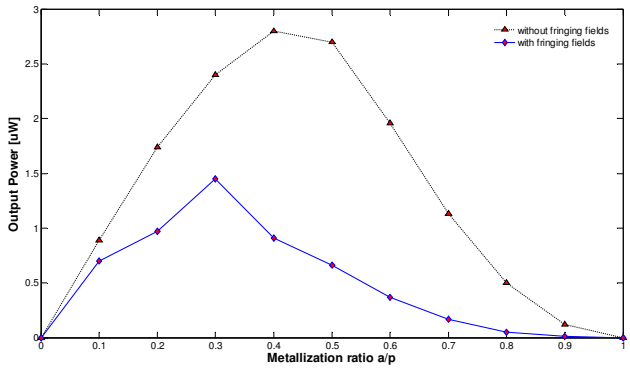

Fig. 7: Output power as a function of metallization ratio a^L/p for a_e=1g, Q_b=2nC, f_0=1200Hz, Q_F=500

CONCLUSION

An approach for capacitance calculation in energy harvesters with strong fringing field effects was presented in detail. An analytical formulation based on the Chebyshev polynomials and the Galerkin method was applied to an electrostatic harvester model with a floating upper electrode that holds a constant charge to provide a bias. In comparison with the parallel plate model, the model with fringing fields has bigger capacitance and induction coefficients but smaller differences between them, leading to lower output power. The optimum operating points are strongly dependent on fringing field effects so these need to be accounted for in device geometry optimization.

ACKNOWLEDGEMENT

This work was supported by The Research Council of Norway under grant no. 191282.

REFERENCES

[1] Mitcheson P D, Sterken T, He C, Kiziroglou M, Yeatmen E M Puers R 2008 Electrostatic microgenerators *Measurement and Control* **41** 114-119

[2] Gladwell G M L, Coen S 1975 A Chebyshev Approximation Method for Microstrip Problems *IEEE Trans. Microwave Theory Tech.* **MTT-23** 865-869

[3] Hashimoto K, Koseki Y, Yamaguchi M 2006 Simulation of Surface Acoustic Wave Devices *Japanese Journal of Applied Physics* **45** 4423-4428

[4] Cuong P L, Einar H 2009 Evaluation of parameters for electrostatic energy harvesters *Technical Digest DTIP 2009 (Rome, Italia, 1-3 April 2009)* 286-291